The 2003 Howe Memorial Lecture
Published with permission of the Iron & Steel Society

Solidification, Segregation, and Banding in Carbon and Alloy Steels

GEORGE KRAUSS

I. INTRODUCTION

STEELS are defined, first and foremost, by their chemistry. For the steel products of interest in this article, steels are defined as alloys of iron, and small amounts of carbon and other chemical elements. In particular, carbon steels are defined as alloys with a maximum of 1.65 wt pct Mn, a maximum of 0.60 wt pct Si, and a maximum of 0.60 wt pct Cu. Maxima in S and P are also specified, but no minimum content of other elements is listed.[1] Alloy steels are steels

Dr. George Krauss is currently University Emeritus Professor at the Colorado School of Mines and a metallurgical consultant specializing in steel microstructural systems. He received the B.S. in Metallurgical Engineering from Lehigh University in 1955 and the M.S. and Sc.D. degrees in Metallurgy from the Massachusetts Institute of Technology in 1958 and 1961, respectively, after working at the Superior Tube Compnay as a Development Engineer in 1956. In 1962–63, he was an NSF Postdoctoral Fellow of the Max Planck Institut für Eisenforschung in Düsseldorf, Germany. He served at Lehigh University as Assistant Professor, Associate Professor, and Professor of Metallurgy and Materials Science from 1963 to 1975, and in 1975, joined the faculty of the Colorado School of Mines as the AMAX Foundation Professor in Physical Metallurgy. He was the John Henry Moore Professor of Metallurgical and Materials Engineering at the time of his retirement from the Colorado School of Mines in 1997.

In 1984, Dr. Krauss was a principal in the establishment of the Advanced Steel Processing and Products Research Center, an NSF Industry –University cooperative research center at the Colorado School of Mines, and served as its first Director until 1993. He has authored the book *Steels: Heat Treatment and Processing Principles*, ASM International, 1990, coauthored the book, *Tool Steels, Fifth Edition*, ASM International, 1998, and edited or coedited conference volumes on tempering of steel, carburizing, zinc-based coatings on steel, and microalloyed forging steels. He has published over 300 papers and lectured widely in technical conferences, universities, corporations, and ASM International Chapters, including a number of keynote, invited, and honorary lectures. He presented the Edward DeMille Campbell Memorial Lecture of ASM International in 2000.

Dr. Krauss has served as the President of the International Federation of Heat Treatment and Surface Engineering (IFHTSE), 1989–91, and as President of ASM International, 1996-97. He is Fellow of ASM International, TMS, and IFHTSE. He has been awarded the Adolf Martens Medal of the German Society for Heat Treatment and Materials, the Charles S. Barrett Silver Medal of the Rocky Mountain Chapter of ASM, the George Brown Gold Medal of the Colorado School of Mines, and several other professional and teaching awards, including the ASM Albert Easton White Distinguished Teacher Award in 1999. He is an Honorary Member of the Iron and Steel Institute of Japan, a Distinguished Member of ISS, and an Honorary Member of ASM International.

"when the maximum of the range given for the alloying elements exceeds one or more of the following percentage limits: Mn 1.65 pct, Si 0.60 pct, Cu 0.60 pct; or in which a definite range or definite minimum quantity of any of the following elements is specified: Al, Cr up to 3.99 pct, Co, Nb, Mo, Ni, Ti, W, V, Zr, or any other element added to obtain a desired alloying effect."[1] Beyond chemistry, steels are also characterized by the steelmaking process used in production (for example, basic oxygen furnace or electric arc furnace), casting process (for example, ingot or continuous casting), size and shape of semifinished products (for example, blooms, billets, or slabs) or finished products (for example, plates, sheet, or bars), or end use or properties.

The chemical definition of steel implies that steels are solid products with uniform chemistry throughout sections of manufactured shapes. While liquid steel at the end of state-of-the-art steelmaking processes is essentially uniform in chemistry,[2] solidification produces macroscopic and microscopic partitioning of chemical elements between parent liquid and growing solid crystals, producing nonuniformity in the distribution of chemical elements inherited in fully solidified as-cast products. This partitioning or segregation of chemical elements occurs on a macroscopic level at the centerline of continuously cast steel products, and at the tops and bottoms, as well as centerlines, of ingots. The effects of macroscopic segregation are outside of the scope of this article. On a microscopic scale, segregation occurs between dendrites throughout a solidified section. The latter segregation is aligned into longitudinal bands by hot rolling, and consequently is referred to as banding, especially when apparent as alternating bands of quite different microstructural constituents. Some degree of banding is found in all types of steel.[1]

Reheating of as-cast products and hot rolling reduce chemical segregation, but further microstructural partitioning, often by design in parent austenite of uniform composition, occurs during diffusion-controlled solid-state phase transformations.[3,4] In view of the dependence of the kinetics of solid-state transformations on chemistry, residual solidification segregation may manifest itself as banding in the microstructure of finished steel products.

The purpose of this article is to review the origins of chemical segregation, and to describe the effects of microsegregation and banding on austenite decomposition, microstructure, and properties of carbon and alloy steels. Banding was of great interest to Henry Marion Howe, and received attention in his classic 1916 text.[5] This article will integrate into the banding literature much more recent results regarding various consequences of banding. Some of those results are based on systematic studies of laminated specimens that simulate microstructures with bands of well-defined differences in chemistry.[6,7,8]

II. DENDRITIC SOLIDIFICATION AND SEGREGATION

Figure 1 is a schematic diagram of the three morphological crystal zones that are typically present in a transverse section of an as-cast shape.[9] The surface zone is referred to as the chill zone and is produced by a high rate of nucleation of fine, randomly oriented, equiaxed crystals in the highly supercooled liquid adjacent to a mold wall. Convection in the liquid adjacent to the chill zone, produced by pouring and temperature differences, may also contribute to the high density of fine crystals in the chill zone.[9] With increasing solidification, a second zone, consisting of columnar crystals, develops. This columnar zone is produced by growth of crystals in preferred crystallographic directions, <100> in the case of body-centered cubic ferrite and face-centered cubic austenite.[11] Constitutional supercooling at the tips of growing crystals promotes the elongated grain shape of the columnar zone.[11] The central zone of an as-cast shape consists of equiaxed crystals. The equiaxed crystals are produced by nucleation in the highly constitutionally supercooled interior liquid, and by breaking off of parts of crystals in the columnar zone by convection in the liquid.[9,10,11]

The equiaxed and columnar crystals shown in Figure 1, by virtue of constitutional supercooling and preferred crystallographic growth, are in fact formed by a mechanism of solidification that produces dendritic or branched, tree-shaped crystals. Figures 2[12] and 3[13] show schematic diagrams that illustrate dendritic crystal solidification and some of the phenomena that accompany dendritic solidification. The dendrites have a major axis that corresponds to the long axis of the columnar grains shown in Figure 1, but also have orthogonal <100> secondary and tertiary branches, as shown in Figures 2 and 3. Figures 4 and 5 show actual tips of dendrite branches, revealed because of shrinkage porosity, that have formed in the equiaxed solidification zone of an as-cast stirred billet of 4140 steel.[14]

Between dendrites and at the tips of dendrite branches in Figure 2, darker shading shows increases in solute content in the liquid around the solidifying dendrites. Figure 3 notes the liquid flow necessary to compensate for shrinkage due to the volume contraction that accompanies solid formation from the liquid. Also shown are deformation that might cause hot tearing, and small volumes of interdendritic shrinkage,

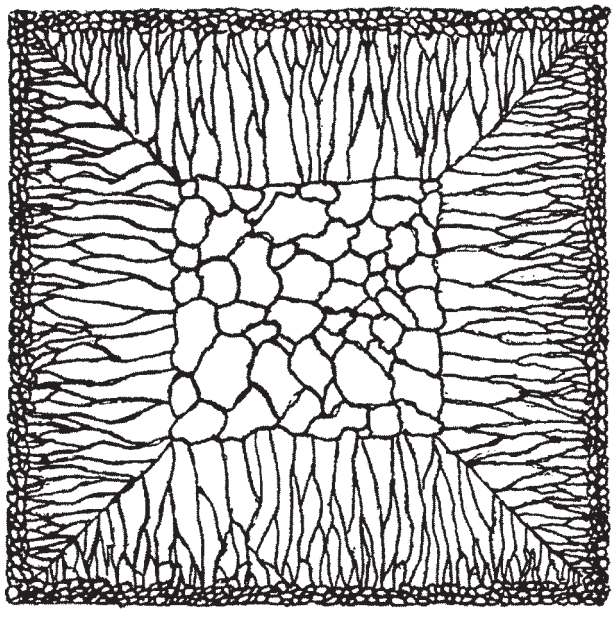

Fig. 1—Schematic diagram of zones of crystal morphologies in an as-solidified section of steel.[9] Shown are the outer chill zone, the columnar zone, and the interior equiaxed zone.

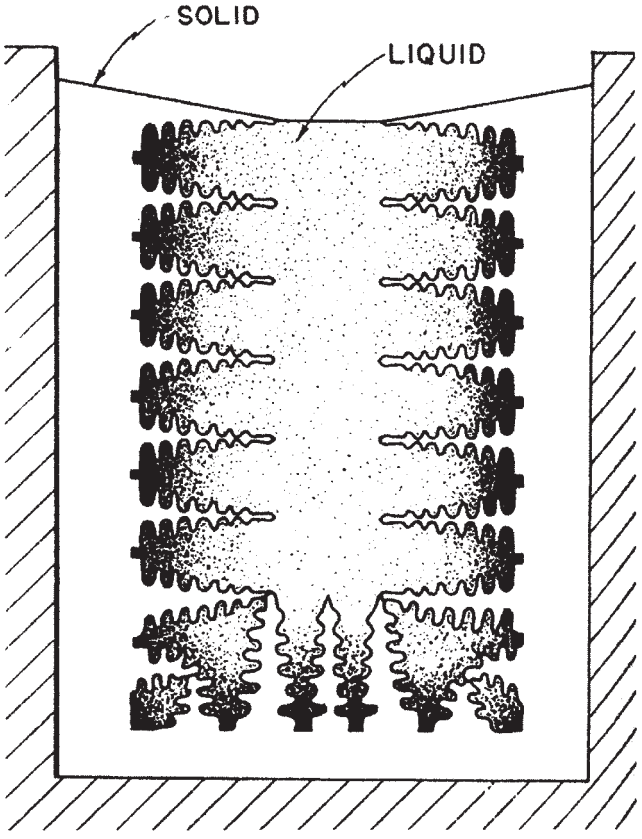

Fig. 2—Schematic of dendritic solidification.[12] The dark shading in liquid adjacent to dendrites represents concentrations of solute atoms rejected from solid.

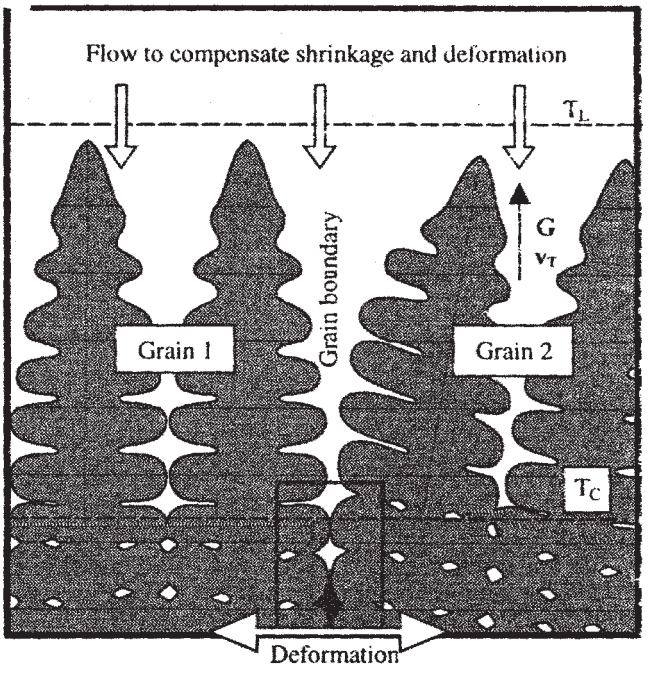

Fig. 3—Schematic of dendritic solidification.[13] Illustrated are liquid convection, effects of deformation, and interdendritic shrinkage where dendrite arms have grown together.

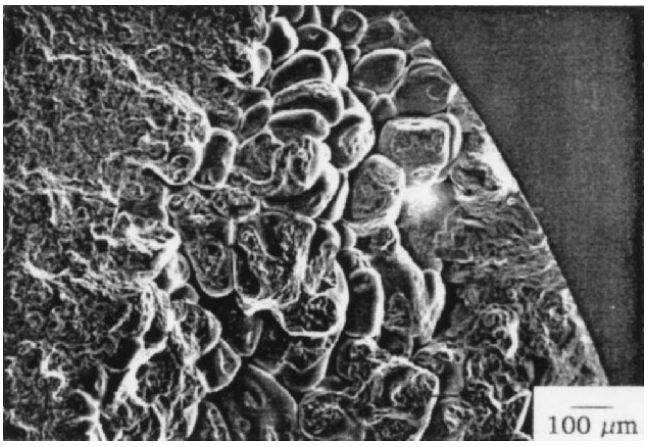

Fig. 4—Dendrite tips at shrinkage porosity in equiaxed solidification zone of an as-cast billet of 4140 steel.[14] SEM micrograph.

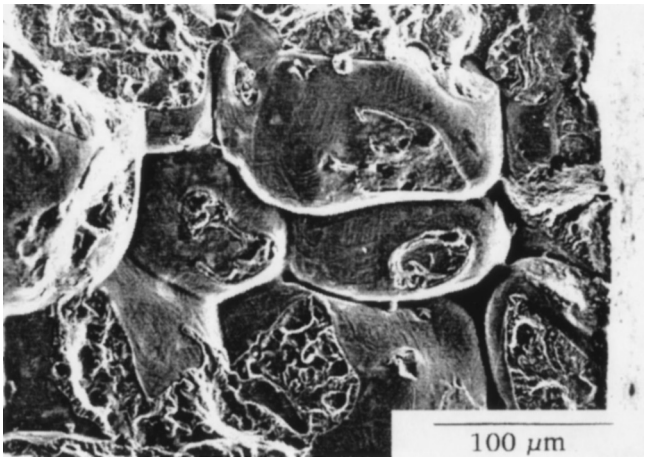

Fig. 5—Another view of dendrite tips at shrinkage porosity in equiaxed solidification zone of an as-cast 4140 steel billet.[14] SEM micrograph.

formed when isolated pockets of liquid solidify after dendrites have grown together. Hot tears that lead to cracking in continuously cast steel billets have been shown to be directly related to dendritic structure, with smooth surfaces conforming to the tips of dendrites.[15] The hot tears form at temperatures close to the solidus where the ductility and fracture strength of steel are near zero. Not illustrated in the schematics of Figures 2 and 3 are the breaking off of dendrite arms, as noted previously, remelting of dendrite tips, dendrite coarsening with increasing distance into the melt, and possible formation of spherical solid particles in the melt by separation from dendrite arms with reduced radii of curvature along their length.[16]

Solute atom redistribution during dendritic solidification is driven by the equilibrium partitioning of chemical elements within the liquid-solid phase field. The two-phase field is defined as a function of temperature by liquidus and solidus curves of the equilibrium phase diagram. At any given temperature, the solute concentration of the solid may be designated as C_S and that of the liquid as C_L, as defined by a tie-line at that temperature. The redistribution or

partitioning of solute is then defined as the equilibrium partition ratio, k, as[10]

$$k = C_S/C_L \quad [1]$$

With this parameter, solute redistribution in the solid C_S as a function of the weight fraction of solid in a volume element, f_s, is given by the Scheil equation as

$$C_S = kC_0(1-f_S)^{k-1} \quad [2]$$

where C_0 is the initial alloy composition within the volume element.[10] The Scheil equation is based on a number of simplifying assumptions, including negligible undercooling, complete diffusion in the liquid in the volume element, negligible diffusion in the solid, and constant k throughout solidification. Other more complicated equations of solute distribution, including the effects of diffusion in the solid and convection, have been evaluated,[10,17] but Eq. [2] accurately demonstrates solute enrichment in the solid as solidification proceeds. The first solid to solidify has the lowest solute content, and the concentration of solute, or solutes in multicomponent alloys such as steels, increases in the solid phase with increasing solidification, with the highest concentration of solutes in the last portion of liquid to freeze.

Table I lists k values, assumed to be independent of temperature, of some elements commonly found in steels.[18] Solute elements with low values of k have the greatest tendency of segregate. Therefore, phosphorus has a very strong tendency to segregate during solidification. However, the amount of the element present is also a factor. Therefore, Mn, generally present in much higher concentrations than P, plays a more important role in segregation and banding than P despite its higher value of k. For a 1.0 pct Mn steel, according to Eq. [1], Mn would vary from 0.70 pct at the beginning of solidification to 1.60 pct at the end of solidification.[18]

Given the facts of dendritic growth and solute redistribution during solidification, the scale of partitioning or segregation is then dependent on the conditions of solidification that determine dendrite size. Frequently, secondary dendrite arm spacing is used as a measure of the scale of interdendritic segregation. Figures 6 through 8 show secondary dendrite arm spacing as a function of various parameters.[10,19–21] Secondary dendrite arm spacing increases with increasing distance from the chill surface, with decreasing cooling rate, and with increasing section size. Thus, continuous casting of smaller section sizes, for example, slabs, thin slabs, and strip, in contrast to the casting of large ingots, is beneficial in reducing the scale of segregation.

Table I. Equilibrium Partition Ratios for Various Elements in Steel[18]

Element	k
P	0.14
Nb	0.23
Cr	0.33
Mn	0.71
Ni	0.83

The size of columnar zones (Figure 1) and associated interdendritc segregation and shrinkage porosity are greatly reduced by the use of in-strand or in-mold electromagnetic stirring.[22] The latter technique effectively increases the size of the equiaxed solidification zone and greatly reduces the amount of centerline shrinkage. The relative size of columnar and equiaxed zones in a cast cross section are also affected by superheating of liquid steel. High superheating in unstirred billets increases the size of the columnar zone because the nucleation of equiaxed dendrites is retarded.[23,24] Figure 9 shows the dramatic effect of small changes in superheat on the relative amounts of columnar and equiaxed solidification zones in continuously cast steel.[25] Electromagnetic stirring reduces the effects of high superheats, but does not completely compensate for the increased size of columnar zones developed by high superheat temperatures.

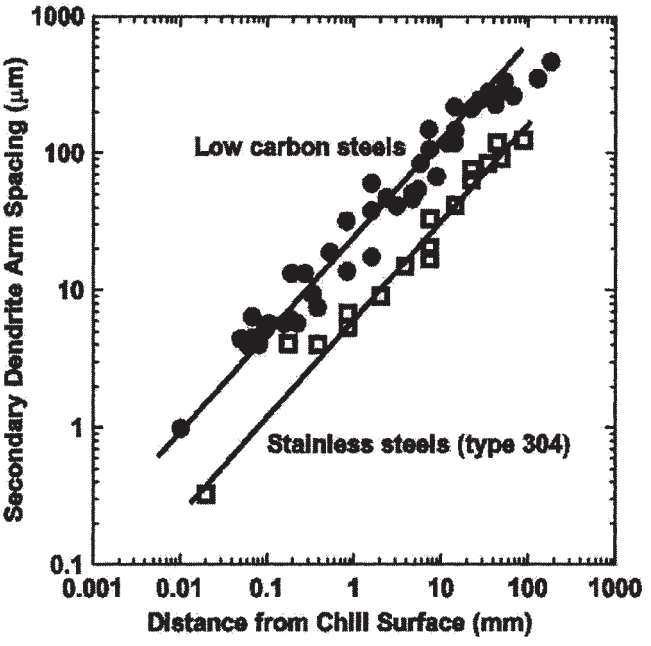

Fig. 6—Secondary dendrite arm spacing as a function of distance from the chill surface of steel from various low-carbon and stainless steel casters. Redrawn from Ref. 19.

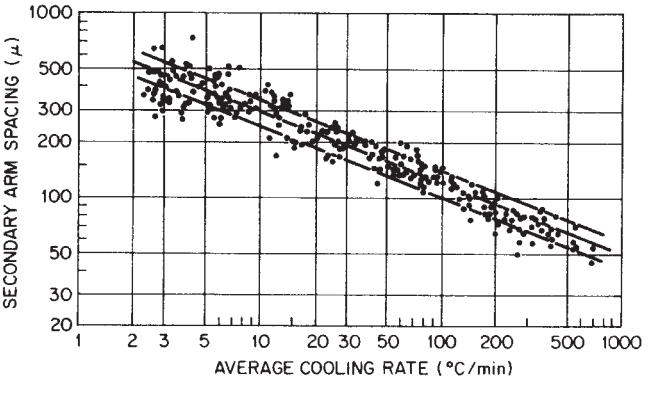

Fig. 7—Secondary dendrite arm spacing as a function of cooling rate for commercial steels containing from 0.1 to 0.9 pct C.[10,20]

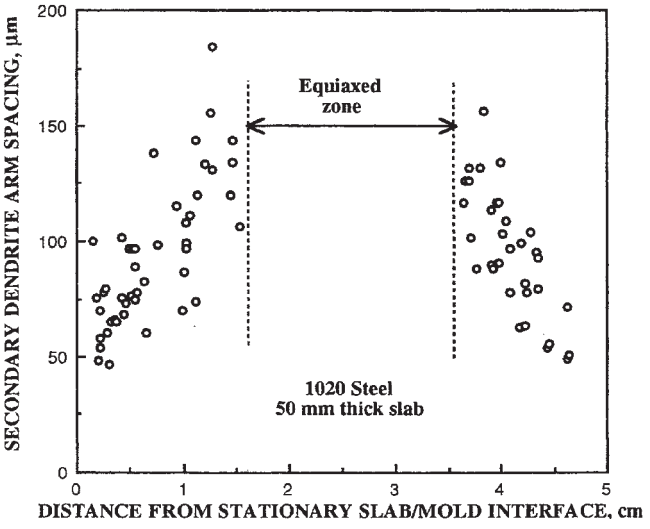

Fig. 8—Secondary dendrite arm spacing as a function of distance across an as-cast slab of 1020 steel.[21]

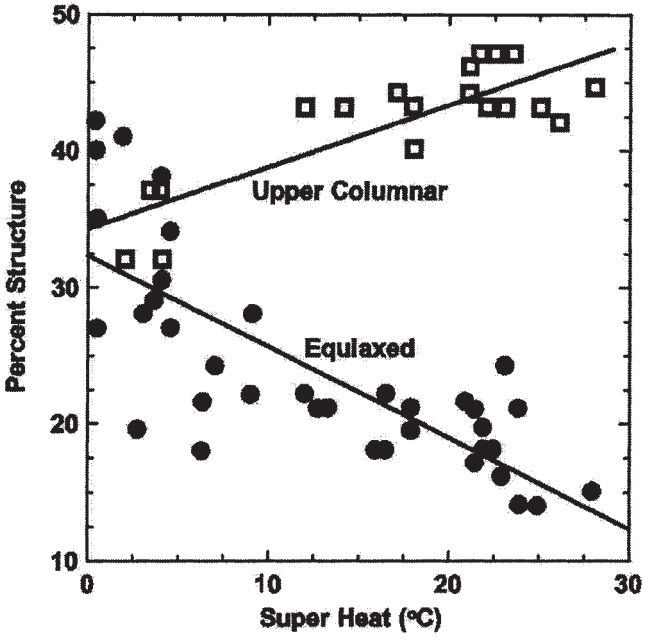

Fig. 9—Percent of as-cast columnar and equiaxed zones as a function of superheat. Redrawn from Ref. 25.

III. HOT WORK AND ITS EFFECT ON SOLIDIFICATION STRUCTURE

As-cast sections, with inclusion contents residual from steelmaking, dendritic microstructures, chemical variations associated with interdendritic segregation, and porosity produced by solidification shrinkage, as described previously, constitute the starting conditions for hot work and the incorporation of banding into steel products. As noted, the smaller the section size, the finer will be the scale of dendritic structure and associated segregation. Therefore, the continuous casting of smaller sections, on the one hand, is beneficial, but on the other hand, does not eliminate banding, because less homogenizing hot work is required to produce finished section sizes. The latter aspect of continuously cast billets, for example, the suitability of hot rolled to bars for forging applications, has been of concern in view of possible detrimental effects of residual solidification effects on properties. A review[26] of the effects of limited hot reduction shows that wrought properties can be established with relatively low hot reduction ratios, typically around 7:1. Therefore, only small as-cast billets with limited reduction to large bars and forgings may be adversely affected by residual solidification structures. With a reasonable degree of hot work, solidification shrinkage is effectively eliminated and dendritic crystals are broken up and recrystallized. Inclusions cannot be removed by hot work, but may be changed in size, morphologies, and distribution by hot work.[27]

Interdendritic chemical segregation is modified, but not eliminated, by typical industrial hot work processing. Figure 10 shows microstructures of transverse sections of bars of 10V45 steel hot rolled from a continuously cast, nonelectromagnetically stirred billet, 178 × 178 mm in section, to bars with diameters of 76, 64, 38, and 29, corresponding, respectively, to reduction ratios of 7:1, 10:1, 27:1, and 49:1.[28] The specimens have been etched with hot picric acid containing sodium trideclybenzene sulfonate, an etch responsive to chemical variations but not to ferrite-pearlite microstructure of the as-rolled bars. Figure 10 shows that the chemistry changes associated with dendritic structures are reduced in size with increasing hot reduction, but are never fully eliminated, even after extensive hot work reduction. The structures revealed in Figure 10 are only the chemical remnants of the as-cast interdendritic segregation and do not correspond to the crystal structures of the as-cooled bars. The dendritic crystals formed on solidification have been replaced successively by transformations on cooling of the as-cast section, by new austenite crystals, formed on reheating and by dynamic and static recrystallization during hot work, and by ferrite-pearlite crystal structures produced by austenite transformation during cooling from finish hot work temperatures. Ferrite-pearlite microstructures superimpose on the chemical variations shown in Figure 10.

Hot rolling aligns the interdendritic variations in chemistry in bands parallel to the rolling direction, producing alternating regions of high and low concentrations of various solute elements. Substitutional elements, with low diffusion coefficients, respond most sluggishly to the homogenizing effects of hot work. With the advent of dedicated electron microprobe analyzers and scanning electron microscopes equipped with wavelength dispersive spectrometers, variations in substitutional element concentrations as a function of distance across longitudinal sections could be quantitatively established.

Figure 11 shows Mn and C concentrations as a function of position across a longitudinal section of a quench and tempered 4140 steel bar, containing by heat analysis 1.00 pct Mn.[29] There is considerable variation in the substitutional element Mn, but only very small variations in the interstitial element C. In view of the high diffusivity of C, it is unlikely that the C variations are residual from the as-solidified structure. The slight carbon variations may in fact be a result of the effect of Mn on the activity of C, as proposed by Kirkaldy *et al.*[30] Manganese lowers the activity of C in austenite, and therefore Mn-rich regions would tend to attract C. Similarly, Cr lowers C activity, while P, Si, and Ni raise

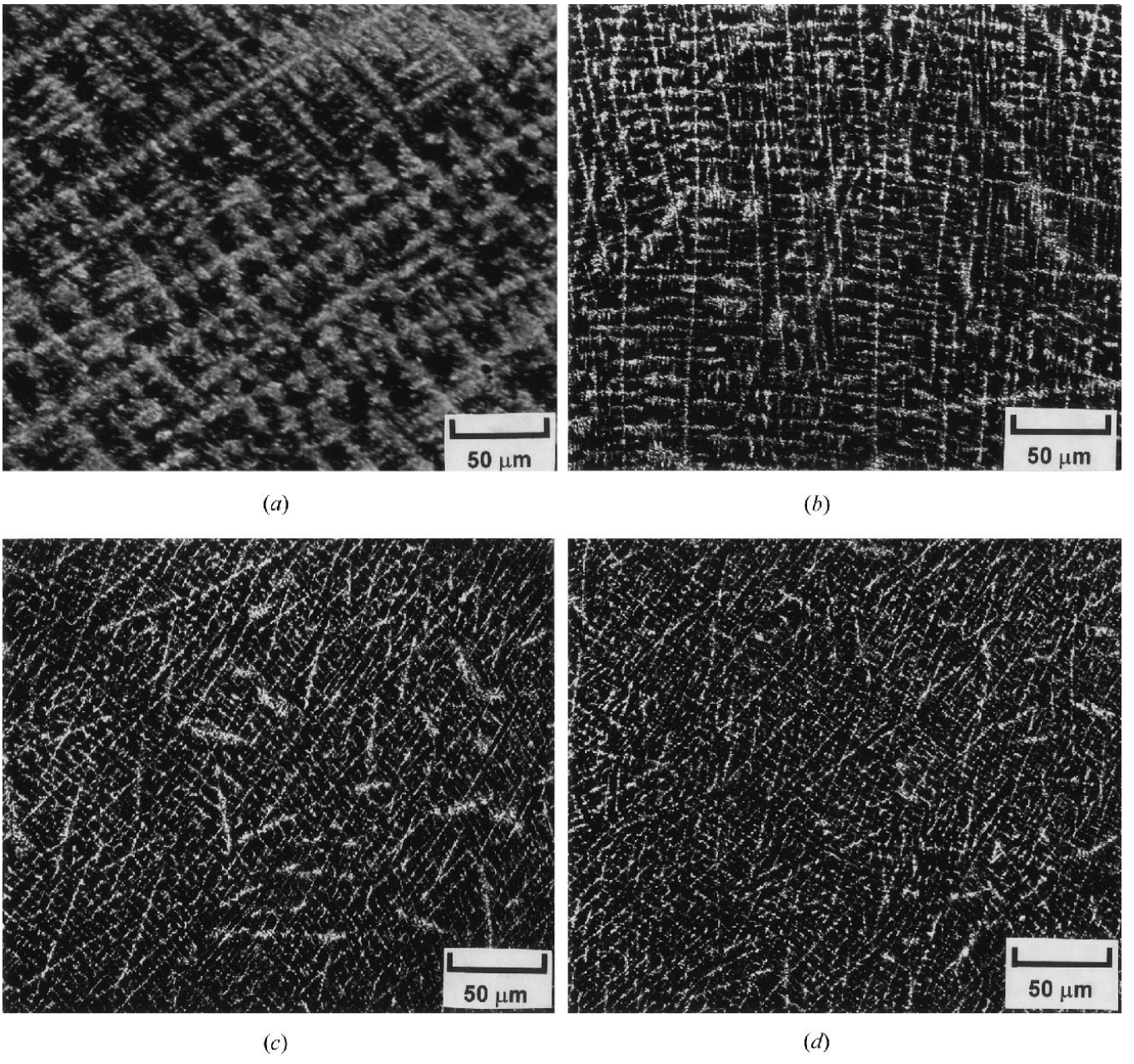

Fig. 10—Remnants of dendritic structure in 10V45 steel hot rolled to reduction ratios of (*a*) 7:1, (*b*) 10:1, (*c*) 27:1, and (*d*) 49:1. Transverse sections, picric acid-sodium tridecylbenzene etch, light micrographs.

C activity, causing rejection of C from regions rich in these elements. Steels, of course, are multicomponent alloys, and all elements segregate to some degree. Figure 12 shows variations in Mn, Cr, and Ni in an 8617 steel bar, containing, by heat analysis, 0.18 pct C, 0.82 pct Mn, 0.52 pct Cr, and 0.44 pct Ni.[29]

The approach to reduced chemical variations created by solidification depends on the scale of the initial dendritic structure, the range of chemical segregation, and the time and temperature of soaking and hot rolling operations. Flemings[10] has published an approach to estimating the effects of the various factors by defining a residual microsegregation parameter, δ, as follows:

$$\delta = (C_M - C_m)/(C^{o}_{M} - C^{o}_{m}) \qquad [3]$$

where C^{o}_{M} and C^{o}_{m} are, respectively, the maximum solute content in the interdendritic space and the minimum solute concentration in the center of the dendrite arm in the as-solidified structure; and C_M and C_m are, respectively, the solute concentrations in the interdendritic space and the center of the dendrite arm after some time, t, at temperature. Residual segregation can then be estimated from

$$\delta = \exp\left[-\pi^2 (D_S\, t/l^2)\right] \qquad [4]$$

where D_S is the solute diffusion coefficient at temperature and l is one-half the dendrite spacing. Fisher *et al.*[18] point out that for a dendrite arm spacing of 300 μm at a temperature of 1250 °C, 35 hours would be required to reduce the segregation of a typical substitutional element by 50 pct.

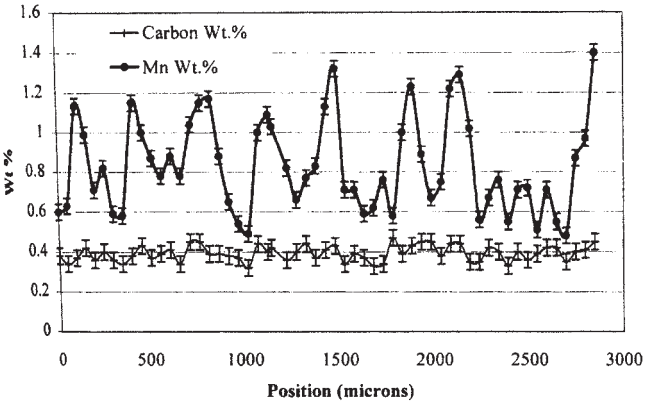

Fig. 11—Variations in Mn and C concentrations across a quench and tempered 4140 steel bar, 95.25 mm in diameter and containing by heat analysis 1.00 pct C.[29] Electron microprobe analysis.

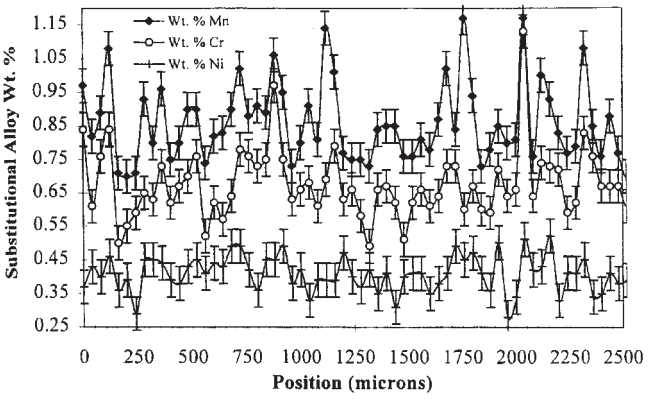

Fig. 12—Variations in Mn, Cr, and Ni across a hot-rolled bar of 8617H steel, 26.19 mm in diameter and containing by heat analysis 0.82 pct Mn, 0.52 pct Cr, and 0.44 pct Ni. WDS SEM analysis.

Experimental studies verify the very long times and high temperatures needed to reduce or eliminate microsegregation,[31] and, although there is a strong movement to casting smaller section sizes, which in turn would have smaller dendrite spacing, the times for complete homogenizing of chemistry are too long for modern steel mill productivity.

IV. BANDED MICROSTRUCTURES

Banding is the microstructural condition in which alternating bands of quite different microstructures, parallel to the rolling direction, develop in steel products, especially in slow-cooled carbon and alloy steels. The root cause of banding is residual interdendritic microsegregation, as discussed previously, and although that segregation is almost always present, the microstructural manifestations of banding may not be present, depending on austenite grain size and cooling conditions that control austenite decomposition to other phases.

Figures 13 and 14 show, respectively, examples of banding in air-cooled bars of 1020 steel[32] and 10V45 steel.[28] The 1020 steel contains 0.22 pct C, 1.04 pct Mn, 0.32 pct Si, and 0.004 pct S, and the microstructure consists of ferrite bands (white) alternating with bands of pearlite (black). The

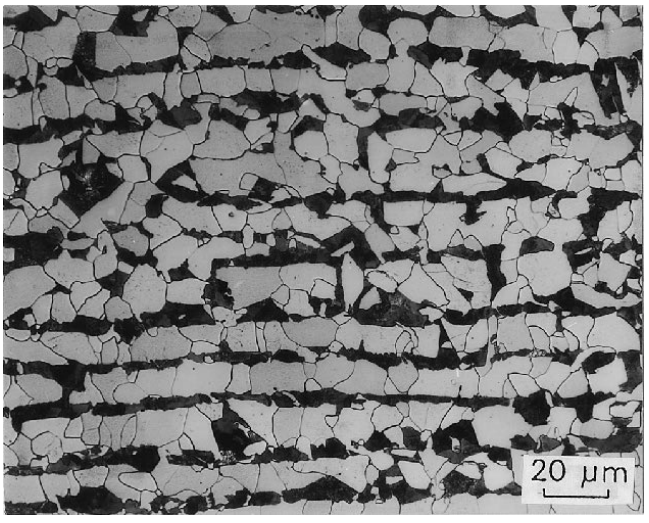

Fig. 13—Ferrite (light) and pearlite (dark) bands in 1020 steel hot-rolled plate. Nital etch, light micrograph.

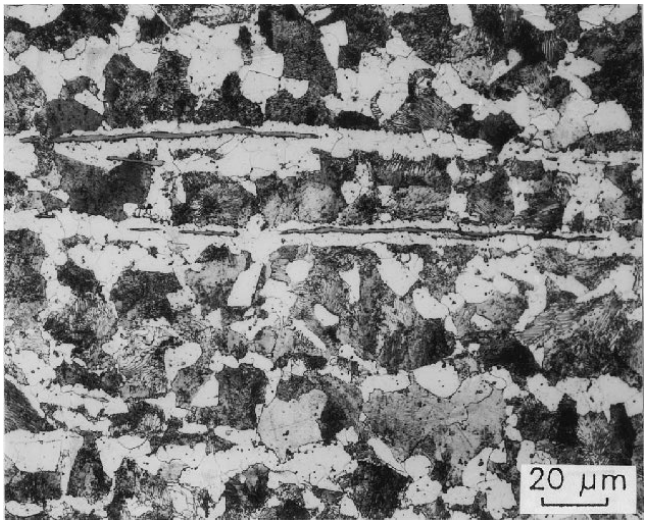

Fig. 14—Ferrite bands with MnS inclusions and pearlite bands in 10V45 steel bar hot rolled to a reduction ratio of 27:1. Longitudinal section, nital etch, light micrograph.

pearlite appears uniformly dark because the ferrite-cementite lamellae of the pearlite are too fine to be resolved in the light microscope. The 10V45 steel contains 0.46 pct C, 0.84 pct Mn, 0.29 pct Si, 0.16 pct V, and 0.029 pct S, and the ferrite-pearlite microstructure has developed in the same bar whose remnant dendritic structure is shown in Figure 10(b). As in the 1020 specimen, in the 10V45 steel, there are alternating bands of ferrite and pearlite, but the ferrite bands are associated with elongated MnS inclusions. Many other good examples of ferrite pearlite banding are included in the text by Samuels.[33]

The pervasive appearance of banding has stimulated considerable literature examination and reviews concerning its origin.[18,30,33–40] Most studies focus on hypoeutectoid steels, but Verhoeven[39] has recently addressed banding in hypereutectoid steels. In hypoeutectoid steels, the ferrite-pearlite banding shown in Figure 13 is explained by the

effect of Mn on the Ar_3 temperature. Manganese stabilizes austenite and lowers Ar_3. Therefore, in a steel with high- and low-Mn bands, on cooling, ferrite forms first in low-Mn bands of the austenite. Carbon is rejected from the ferrite as it grows, concentrating in the high-Mn regions where pearlite eventually forms. This process is illustrated in an article by Thompson and Howell,[40] who point out the importance of austenitic grain size. When the austenitic grain size is smaller than the wavelength of microsegregation, ferrite grains nucleate on austenite grain boundaries and triple points in Mn-poor regions with high Ar_3 temperatures. These grains impinge or grow together in the rolling direction, and then proceed, with common boundaries transverse to the rolling direction, to grow toward Mn-rich regions. A "bamboo" ferritic grain structure therefore is often produced by ferrite nucleation and growth between pearlite bands. Austenitic grain sizes greater than the wavelength of segregation result in the disappearance of banding. Also, in hardenable steels, cooled at high enough rates to transform both low and high solute regions to martensite, no microscopic evidence for banding is produced, except for possible small differences in etching behavior of the martensitic structures.

A quite different mechanism explains the banding of the 1045 steel (Figure 14), where the ferrite has formed around elongated MnS inclusions. Interdendritic segregation concentrates both Mn and S and thereby results in the formation of MnS inclusions. However, after hot work, Kirkaldy *et al*.[37] show that Mn concentrates in MnS with decreasing temperatures in the austenite phase field, depleting initially high-Mn regions around the MnS inclusions of Mn. Therefore, ferrite nucleation and growth occur in regions with initially high interdendritic concentrations of Mn. Carbon is rejected from ferrite and thus pearlite in the 10V45 steel forms in low-Mn bands in contrast to its formation in high-Mn bands in low-sulfur steels.

V. THE EFFECT OF BANDING ON MECHANICAL PROPERTIES

The presence of banding has stimulated numerous investigations of the effects of banding on mechanical behavior of steel. Owen *et al*.[41] compared the behavior of low-carbon steel with banded and homogenized microstructures and found no difference in impact properties below the transition temperature. However, in the testing temperature range for ductile fracture, both longitudinal and transverse energy absorption were higher in homogenized specimens. Grange[42] studied a split heat of 0.25 pct C steel, with one part of high purity and the other with S and Si additions that produced high densities of inclusions. Specimens with and without banding were subjected to tensile and impact testing. In the clean steel, ductile fracture and anisotropy due to banding were markedly improved by homogenization, but only modest improvements by homogenization were achieved in the specimens with high densities of elongated inclusions. Thus, the Grange study underscores the importance of inclusion control for optimized mechanical properties and fracture resistance in steels. Also, bands of martensite, when present in banded specimens, were judged to be deleterious to machining and cold forming operations.

Spitzig[43] studied banding and the effects of inclusions on mechanical properties of a series of 0.2 pct C, 1.0 pct Mn steels with either 0.004 or 0.013 pct S. Again inclusions dominated anisotropy and degradation of mechanical properties and banding was found to have no effect on reduction of area or Charpy shelf energies in any of the steels. Improvement in properties produced by a high-temperature treatment (10 minutes at 1315 °C) that eliminated banding was shown to be a result of coarsening or reduction in aspect ratios of inclusions rather than the elimination of banding.

Studies of banding have typically only examined a limited number of banded states, and the wavelength of microsegregation and banding may vary significantly within a given steel. For example, in the Thompson and Howell study,[40] the average banding wavelength was 60 μm and ranged from about 20 to 120 μm. The chemical gradients due to interdendritic segregation are also variable, and concentrations of solutes vary continuously between high and low values, as influenced by mill-dependent reheating and hot work processing. In order to systematically evaluate extreme effects of banding, *i.e*., effects on microstructure and tensile properties associated with well-defined, nonhomogenized chemical gradients, a recent study has evaluated artificially banded steel specimens.[6,7,8] Band spacings and cooling rate were systematically varied. A detailed description of the design and selected results of that study follows.

Table II lists the chemistry of the SAE 5140 steel, a representative medium-carbon, low alloy steel, and the chemistry of the modification of the 5140 steel, used to produce artificially banded specimens. The two steels differed only in Mn content, 0.82 pct for the 5140 steel and 1.83 for the modified 5140M steel. The steels were vacuum induction melted, rolled to plate, and homogenized in vacuum for 12 hours at 1300 °C. Cleaned, cold-rolled sheets of the steels, 0.50-mm thick were stacked in 200 sheet packets and hot and cold rolled to specimens with band thicknesses of 320, 160, 80, 40, and 20 μm. Other details of the production of the laminated specimens are presented in References 6 through 8. Sheet tensile specimens of the artificially banded steels with a gage cross section of 6.350×3.175 mm were austenitized at 850 °C for 20 minutes and cooled at rates of 83 °C/s, 5.1 °C/s, 2.6 °C/s, 0.6 °C/s, 1 °C/min, and 0.5 °C/min. The cooling rates were calculated from the rates between 704 °C and 538 °C. Specimens were not tempered after cooling.

Figure 15, calculated with the aid of Thermo-Calc,[44] shows the remarkable difference in cooling transformations and hardenability between the high- and low-Mn 5140 steels. For example, at a relatively low rate of cooling, the low-Mn

Table II. Chemistries (Weight Percent) of Steels Used to Produce Artificially Banded Samples

Steel	C	Mn	P	S	Si	Cu	Ni	Cr	Mo	Al
5140	0.39	0.82	0.014	0.022	0.22	0.16	0.17	0.81	0.04	0.030
5140M	0.41	1.83	0.015	0.024	0.22	0.16	0.17	0.81	0.04	0.029

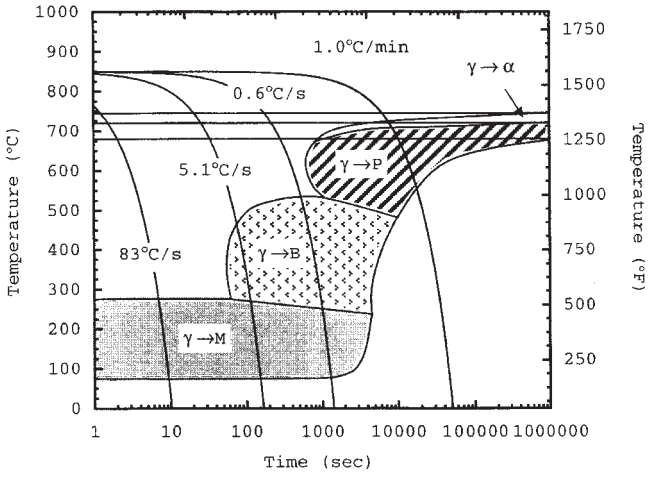

(*a*)

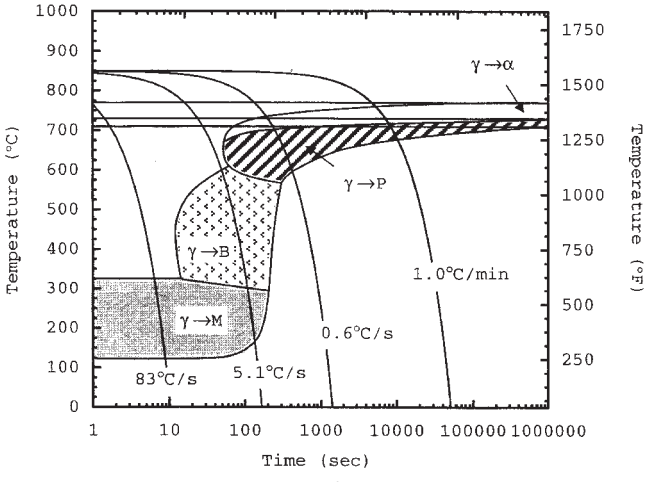

(*b*)

Fig. 15—Continuous cooling transformation diagrams for 5140 steel containing (*a*) 1.83 Mn and (*b*) 0.82 pct Mn.[6]

5140 steel would be completely transformed to a microstructure of ferrite and pearlite, while the high-Mn 5140M steel would be transformed primarily to bainite and small amounts of martensite. Figure 16 confirms these differences in transformation and microstructure. Shown are the microstructures of laminated specimens with the various band spacings. The bainitic regions appear gray, the ferrite-pearlite regions consist of a mix of white (ferrite) and black (pearliite) features, and fully pearlitic areas appear black. As indicated in the CCT diagrams, the high-Mn bands consist completely of bainite and the low-Mn bands consist entirely of ferrite and pearlite.

A striking feature of the banded microstructures (Figure 16) is the fully pearlitic band that appears to separate the high- and low-Mn bands of the laminated specimens. This band has been shown[8] to result from carbon rejection into the high-Mn layer from the first ferrite formed in the low-Mn bands. A continous layer of pearlite forms, and grows into the high-Mn layer. In view of the constant cooling conditions, the growth of the pearlite is limited by carbon diffusion, to a thickness of 20 to 30 μm, in all of the specimens. Thus, in the specimens with the largest bandwidth, the pearlite band is only a small fraction of the microstructure, while in the specimen with the finest band spacing of 20 μm, the pearlite has grown to the full width of the high-Mn band, and occupies one half of the microstructure.

Figure 17 shows engineering stress-strain curves for specimens with all band spacings after cooling at 83 °C/s, 5.1 °C/s, 0.6 °C/s, and 1.0 °C/min. All the specimens quenched at 83 °C/s, a rate achieved by an oil quench, transformed to martensite in both the high- and low-Mn bands and showed no evidence of banding except for a slight etching difference. However, all of the rapidly cooled specimens were brittle, a result shown to be caused by intergranular fracture at prior austenite grain boundaries of the high-Mn bands.[6,8] The fracture morphology of the low-Mn martensite was ductile, characterized by microvoid formation and coalescence. Thus, high Mn has caused quench embrittlement of the 5140 steel, an embrittlement mechanism of hardened medium- and high-carbon steels attributed to P segregation and cementite formation at austenite grain boundaries during austenitizing or cooling from austenitizing temperatures.[45] This effect of Mn on susceptibility to quench embrittlement has not been demonstrated heretofore, and may be related to the effect of Mn on the activity of C. As proposed by Kirkaldy *et al.*,[30] Mn lowers the activity of C in austenite and stimulates C diffusion to high-Mn areas, perhaps at austenite grain boundaries and certainly at the interfaces of the low- and high-Mn bands. Such enhanced carbon diffusion may promote the cementite formation that has been associated with quench embrittlement. Tempering of the artificially banded specimens after quenching would reduce or eliminate the effects of quench embrittlement.[46]

The tensile loading behavior of laminated specimens cooled at intermediate rates (Figures 17(b) and (c)) shows the greatest sensitivity to banding spacing, a result caused by the various layered mixtures of bainite, ferrite, and pearlite formed in response to Mn variations. Specimens cooled at the lowest rates (Figure 17(d)) show high uniformity in mechanical behavior because of complete transformation to ferrite and pearlite microstructures in both the high- and low-Mn bands.

VI. SUMMARY

Sections II through V have followed the origin of banding, from the formation of as-cast dendritic structures and associated interdendritic segregation, through to microstructures with well-defined alternating bands of various microstructures, formed after cooling from hot-rolled austenite with bands of varying alloy content and inclusions. The extent of banding, derived from the aligned residual interdendritic segregation, is very much alloy, section size, and mill processing dependent, and dramatic variations in the effects of banding can develop, depending on banding severity and cooling conditions. The effects of banding may or may not be detrimental to finished steel products or their production, and if questions arise, banding and its effects merit appropriate evaluation.

The artificially banded or laminated specimens described previously illustrate not only factors that control extremes in microstructures and properties of banded steels, but also

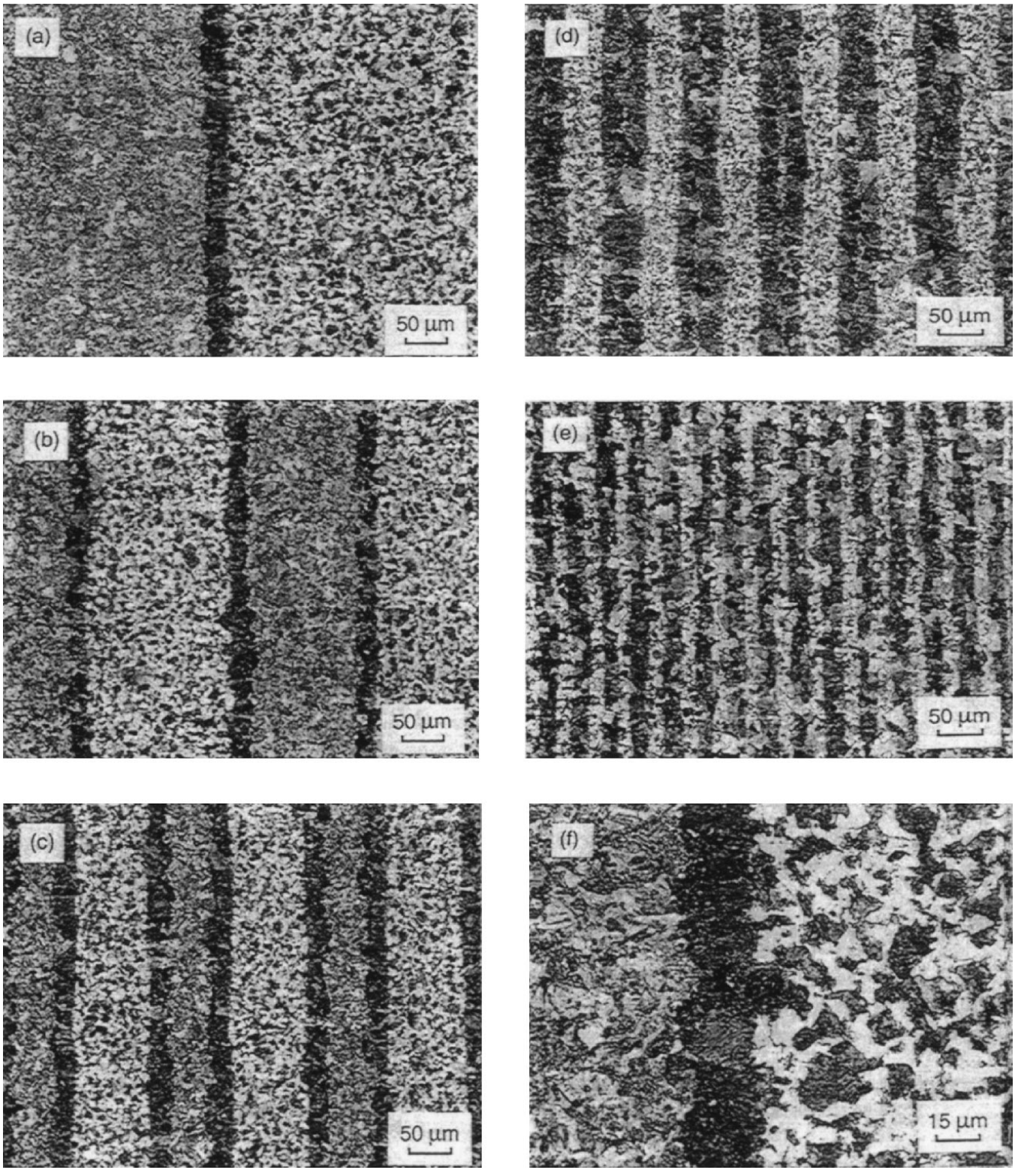

Fig. 16—Microstructures of 5140 steel with band spacings of (*a*) 320, (*b*) 160, (*c*) 80, (*d*) 40, and (*e*) 20 μm, after cooling at 0.6 C/s. (*f*) The interface of 320-μm bands at higher magnification. Bands with 1.83 pct Mn contain bainite (gray) and pearlite (dark). Bands with 0.82 pct Mn contain a mixture of ferrite and pearlite (mixed white and black). Nital etch, light micrographs.

show that lamination can produce engineered steel products with well-defined layers of quite different chemistry and microstructure. In fact, banding in high-carbon steels has produced the great utility and beauty of Damascus swords made from high-carbon, hypereutectoid steels. Verhoeven[39] has shown that the striking surface textures of Damascus swords are due to etching differences of alternate bands of dispersed carbide particles and pearlite. The hypereutectoid

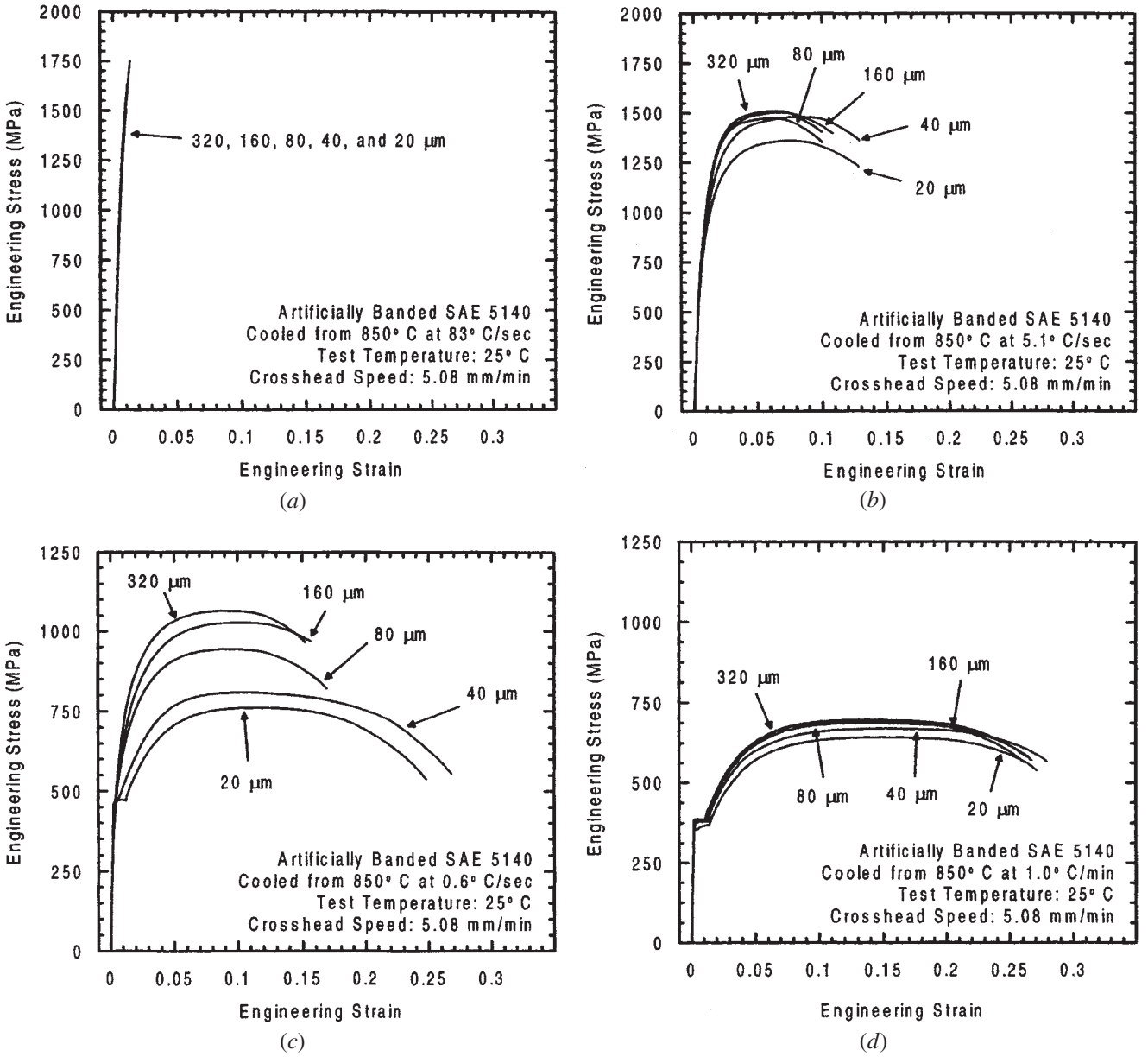

Fig. 17—Engineering stress-strain curves for artificially banded 5140 steel with various band spacings after cooling at (*a*) 83 °C/s, (*b*) 5.1 °C/s, (*c*) 0.6 °C/s, and (*d*) 1.0 C/min.[6]

steel banding requires small amounts of carbide-forming elements such as V or Mo. The latter elements segregate in interdendritic regions and eventually stabilize banded arrays of spheroidized carbide particles in austenite. The spheroidized carbide particles in turn nucleate divorced eutectoid transformation products, *i.e.*, structures of ferrite and dispersed cementite particles, rather than lamellar eutectoid transformation to pearlite in regions free of dispersed carbides. Also, a recent review,[47] recognizing the major contributions of Professor Oleg Sherby, describes the evolution of ultrahigh carbon steels, and lists many ancient and modern applications of laminated composites of high-carbon and low-carbon steels. The effectiveness of such laminated composites in improving fracture toughness is attributed to delamination of weakly bonded layer interfaces.

Future steel products could be highly engineered by even wider use of laminate technology than used to date. Strip casting, with its fine, as-cast dendritic structure, would provide an excellent source of sheets for multilayer laminations. Needless to say, a vast amount of technological development and evaluation would be required to widely exploit the potential of large-scale laminated, artificially banded steel products.

ACKNOWLEDGMENTS

I am deeply honored to have been selected to deliver the 2003 Howe Memorial Lecture and the opportunity to prepare this article. The interest in banded steel structures continues to this day, and requires an integrated approach, spanning

the entire range of steel production from steelmaking to final finished products. The recent related work at the Colorado School of Mines, including especially that of Charles V. White,[25] a Visiting Professor from Kettering University, and students Eric Schultz,[14] Jeff Dyck,[28] Jared Black,[29] and Ted Majka,[6,7,8] was stimulated by the representatives of the sponsor corporations of the Advanced Steel Processing and Products Research Center (ASPPRC), a University/Industry Cooperative Research Center at the Colorado School of Mines. Sponsors of ASPPRC include both corporations that make and use steel, and their support is gratefully acknowledged. I also acknowledge with pleasure the major contributions of my colleague, Professor David K. Matlock, Colorado School of Mines, to the ASPPRC programs referenced in this paper.

REFERENCES

1. *Steel Bar Product Guidelines*, ISS, Warrendale, PA, 1994, pp. 7-10.
2. *The Brimacombe Memorial Symp*., Canadian Institute of Mining, Metallurgy and Petroleum, Montreal, 2000.
3. W.C. Leslie: *The Physical Metallurgy of Steels*, Tech Books, New York, NY, 1981.
4. G. Krauss: *Steels: Heat Treatment and Processing Principles*, ASM INTERNATIONAL, Materials Park, OH, 1990.
5. H.M. Howe: *The Metallography of Steel and Cast Iron*, McGraw-Hill, New York, NY, 1916, pp. 556-65.
6. T.F. Majka: Master's Thesis, Colorado School of Mines, Golden, CO, 2000.
7. T.F. Majka, D.K. Matlock, G. Krauss, and M.T. Lusk: *42nd MWSP Conf. Proc*., ISS, Warrendale, PA, 2000, pp. 75-87.
8. T.F. Majka, D.K. Matlock, and G. Krauss: *Metall. Mater. Trans. A*, 2002, vol. 33A, pp. 1627-37.
9. T.F. Brower and M.C. Flemings: *Trans. TMS-AIME*, 1967, vol. 239, pp. 216-17.
10. M.C. Flemings: *Solidification Processing*, McGraw-Hill, Inc., New York, NY, 1974.
11. R.E. Reed-Hill: *Physical Metallurgy Principles*, 2nd ed., D. Van Nostrand Company, New York, NY, 1973, pp. 568-608.
12. M.C. Flemings and G.E. Nereo: *Trans. TMS-AIME*, 1967, vol. 239, pp. 1449-61.
13. M. Rappaz, I. Farup, and J.-M Drezet: *Proc. Merton C. Flemings Symp*., R. Abbaschian, H. Brody, and A. Mortensen, eds., TMS, Warrendale, PA, 2001, pp. 213-28.
14. E.J. Schultz, J.J. Moore, G. Krauss, D.K. Matlock, R. Frost, and J. Thomas: *34th Mechanical Working and Steel Processing Proc*., ISS, Warrendale, PA, 1992, vol. XXX, pp. 309-19.
15. I.V. Samarasekera: *The Brimacombe Memorial Symp*., Canadian Institute of Mining, Metallurgy and Petroleum, Montreal, pp. 399-419.
16. T.Z. Kattamis and P.W. Voorhees: *Proc. Merton C. Flemings Symp*., R. Abbaschian, H. Brody, and A. Mortensen, eds., TMS, Warrendale, PA, 2001, pp. 119-28.
17. H.D. Brody and M.C. Flemings: *Trans. AIME*, 1966, vol. 236, pp. 615-24.
18. R.M. Fisher, G.R. Speich, L.J. Cuddy, and H. Hu: *Proc. Darken Conf. "Physical Chemistry in Metallurgy,"* US Steel, Monroeville, PA, 1976, pp. 463-88.
19. A.W. Cramb: *Casting of Near Net Shape Products*, TMS, Warrendale, PA, 1988, pp. 673-82.
20. A. Suzuki, T. Suzuki, Y. Nagaoka, and Y. Iawata: *J. Jpn. Inst. Met*., 1968, vol. 32, pp. 1301-05.
21. E. Essadiqi, L.E. Collins, M.T. Shehata, and L.K. Chiang: *2nd Canada–Japan Symp. on Modern Steelmaking and Casting Techniques*, J.J. Jonas, J.D. Boyd, and N. Sano, eds., Canadian Institute of Mining, Metallurgy, and Petroleum, Montreal, 1994, pp. 251-64.
22. T. Emi: *The Brimacombe Memorial Symp*., Canadian Institute of Mining, Metallurgy and Petroleum, Montreal, 2000, pp. 23-38.
23. D.J. Hurtuk: *Proc. Int. Conf. on Solidification*, The Metals Society, London, 1979, pp. 21-29.
24. F. Fattorini and B. Grifoni: Final Report Contract No. 7210-EB/402 (1.7.1985-30.6.1988), European Commission, 1990.
25. W.R. Irving and D.V. Barradell: in *Process Control in the Steel Industry*, G. Carlsson and H. Nordberg, eds., Uddeholm Research, Haggfors, Sweden, 1986, pp. 7-53.
26. C.V. White, G. Krauss, and D.K. Matlock: *Iron Steelmaker*, 1998, vol. 25, No. 9, pp. 73-79.
27. W.C. Leslie: *Trans. ISS*, 1983, vol. 2, pp. 1-24.
28. J. Dyck, R.H. Frost, D.K. Matlock, G. Krauss, W.E. Heitmann, and D. Bhattacharya: *Mechanical Working and Steel Processing Proceedings*, ISS, Warrendale, PA, 1988, pp. 83-94.
29. J. Black: Master's Thesis, Colorado School of Mines, Golden, CO, 1998.
30. J.S. Kirkaldy, J. von Destinon-Forstmann, and R.J. Brigham: *Can. Met. Q*., 1962, vol. 1, pp. 59-81.
31. R.G. Ward: *J. Iron Steel Inst*., 1965, vol. 203, pp. 930-32.
32. Y. Sawada, R.P. Foley, S.W. Thompson, and G. Krauss: *35th MWSP Conf. Proc*., ISS-AIME, Warrendale, PA, 1994, vol. XXXI, pp. 263-86.
33. L.E. Samuels: *Light Microscopy of Carbon Steels*, ASM INTERNATIONAL, Materials Park, OH, 1999, pp. 110-24.
34. P.G. Bastien: *J. Iron Steel Inst*., 1957, vol. 187, pp. 281-91.
35. C.F. Jatczak, D.J. Girardi, and E.S. Rowland: *Trans. ASM*, 1956, vol. 48, pp. 279-303.
36. E.T. Turkdogan and R.A. Grange: *J. Iron Steel Inst*., 1970, vol. 20B, pp. 482-94.
37. J.S. Kirkaldy, R.J. Brigham, H.A. Domian, and R.G. Ward: *Can. Metall. Q*., 1963, vol. 2, pp. 233-41.
38. R. Grossterlinden, R. Kawalla, U. Lotter, and H. Pircher: *Steel Res*., 1992, vol. 63, pp. 331-36.
39. J.D. Verhoeven: *J. Mater. Eng. Performance*, 2000, vol. 9, pp. 286-95.
40. S.W. Thompson and P.R. Howell: *Mater. Sci. Technol*., 1992, vol. 8, pp. 777-84.
41. W.S. Owen, M. Cohen, and B.L. Averbach: *Welding J. Welding Res. Suppl*., 1958, pp. 368s-374s.
42. R.A. Grange: *Metall. Trans*., 1971, vol. 2, pp. 417-26.
43. W.A. Spitzig: *Metall. Trans. A*, 1983, vol. 14A, pp. 271-82.
44. B. Sundman, B. Jansson, and J.O. Anderson: *CALPHAD (Calculation of Phase Diagrams) A Comprehensive Guide*, Elsevier Science, New York, NY, 1985, pp. 153-90.
45. R.S. Hyde, D.K. Matlock, and G. Krauss: *40th MWSP Conf. Proc*., ISS, Warrendale, PA, 1998, pp. 921-28.
46. G. Krauss: *Metall. Mater. Trans. A*, 2001, vol. 32A, pp. 861-77.
47. J. Wadsworth: in *Deformation, Processing, and Properties of Structural Materials*, E.M. Taleff, C.K. Syn, and D.R. Lesuer, eds., TMS, Warrendale, PA, 2000, pp. 3-24.